Geoderma 405 (2022) 115445

Contents lists available at ScienceDirect

Geoderma

journal homepage: www.elsevier.com/locate/geoderma

Micro-analytical study of the distribution of iron phases in ferromanganese nodules

Péter Sipos [a,*], Ivett Kovács [a], Réka Balázs [a], Adrienn Tóth [b], Gyöngyi Barna [c], András Makó [c,d]

[a] Institute for Geological and Geochemical Research, Research Centre for Astronomy and Earth Sciences, Eötvös Loránd Research Network, H1112 Budapest, Budaörsi út 45., Hungary
[b] Geographical Institute, Research Centre for Astronomy and Earth Sciences, Eötvös Loránd Research Network, H1112 Budapest, Budaörsi út 45., Hungary
[c] Institute for Soil Sciences, Centre for Agricultural Research, Eötvös Loránd Research Network, Eötvös Loránd Research Network, H1022 Budapest, Herman Ottó út 15., Hungary
[d] Georgikon Campus, Magyar Agrár- és Élettudományi Egyetem, H8360 Keszthely, Deák Ferenc út 16., Hungary

ARTICLE INFO

Handling Editor: David Laird

Keywords:
Hydromorphic soils
Concentric nodules
Typic nodules
Micro-fabric
Goethite
micro-XRD

ABSTRACT

The differentiation of Fe and Mn within the nodules and its relation to the fabric is a well-known phenomenon. However, the relationship of this differentiation to the nodules mineralogy was not studied yet. This study aimed to fill this gap through the micro-mineralogical and geochemical investigation of nodules from soils with different hydromorphic conditions by electron probe microanalysis and micro-X-Ray diffractometry.

Different conditions of hydromorphism resulted in the same nodule types and their similar vertical distribution in soils. In soils with shallow groundwater table, nodules exhibited more developed fabric, and crystalline hydrous Fe oxides (goethite) prevailed in them. Contrarily, nodules showed smaller size, lower Fe enrichment, and a higher frequency of non-crystalline hydrous Fe oxides in soils with regular flooding and stagnant surface water. The difference could be related to the lower intensity of water oscillation and the shorter redox periods in the latter soils. The formation of the nodules' fabric may have been followed by the slow crystallization of Fe-oxyhydroxides when favorable redox oscillation conditions occur allowing subsequent recrystallization. The association of hydrous Fe oxides to clay minerals may have also affected the crystallization process within the nodules.

Although the observation of assumed differentiation of hydrous Fe oxides failed within the nodules, soils with different conditions of hydromorphism could be characterized by different Fe-oxyhydroxide mineralogy, at least in the progression of their crystallization process.

1. Introduction

Ferromanganese nodules are hard bodies made of soil particles cemented by (hydrous) Fe and Mn oxides. Their formation is a common phenomenon in soils with impeded internal drainage (Vepraskas and Vaughan, 2016). Nodules represent morphological features with large heterogeneity even from the same soil horizon: they may vary widely in size, color, shape, and fabric, thus reflecting different and/or changing pedogenic conditions (Gasparatos et al., 2019). Frequently alternating water regimes may result in varying redox potential in the different parts of the soil, at the surface of, and within the nodules at the same time. Consequently, diverse dissolution, precipitation, and diffusion processes may proceed regarding Fe and Mn in the soil and within the nodules (White and Dixon, 1996; Palumbo et al., 2001; Cheng et al., 2009).

The primary Fe phase forming upon rapid oxidation of Fe^{2+} is weakly crystalline ferrihydrite. This phase slowly transforms to thermodynamically more stable minerals (Cornell and Schwertmann, 2003; Thompson et al., 2006). However, the crystallization process might be interrupted. Even small amounts of organic matter can influence the ferrihydrite's particle size and structural order, resulting in smaller crystals, increased lattice spacing, and distorted $Fe(O,OH)_6$ octahedral (Eusterhues et al., 2008). Several studies showed (Kölbl et al., 2014; Vogelsang et al., 2016; Chen et al., 2019) that short-range ordered Fe minerals were often formed during the oxidative precipitation at the oxic/anoxic interface in temporarily drained topsoil, likely because of the high organic matter content. Conversely, Fe phases formed in the subsoil were typically more crystalline, probably due to the longer persistence of dissolved Fe(II), which catalyzed the re-crystallization of precipitated hydrous Fe oxides.

* Corresponding author.
E-mail address: sipos.peter@csfk.org (P. Sipos).

https://doi.org/10.1016/j.geoderma.2021.115445
Received 8 March 2021; Received in revised form 25 August 2021; Accepted 29 August 2021
Available online 7 September 2021

The higher crystallinity of these phases in the subsoil may also suggest a different timescale of Fe redox cycling (Chen et al., 2019). Other conditions, like pH, dissolved ions (Si, Al), and microbial activity, also influence the formation and crystallization of hydrous Fe oxides (Cornell and Schwertmann, 2003; Jones et al., 2009; Bonneville et al., 2009).

Nodules can be characterized by variable (hydrous) Fe oxide mineralogy: goethite, hematite, lepidocrocite, and ferrihydrite are their most common Fe minerals (e.g., Rhoton et al., 1993; Cornu et al., 2005; Szymanski et al., 2014). The differentiation of Fe and Mn within the nodules and its relation to the fabric is a well-known phenomenon (Gasparatos et al., 2005; Hickey et al., 2008; Sun et al., 2018). These results raise the question of whether there is a similarly large variation within the nodules' mineralogy. Using synchrotron-based techniques, Manceau et al. (2003) found that the Fe-rich outer zone of a studied nodule could be characterized by goethite solely, whereas its Fe-Mn-rich nucleus by feroxyhite, vernadite, and only minor goethite. Further studies on the nodules' mineralogy used bulk methods exclusively (e.g. Zhang and Karathanasis, 1997; Ram et al., 2001; Aide, 2005; Yu and Lu, 2016; Sun et al., 2018; Šegvić et al., 2018), which are not useful to study the mineralogical variance within nodules. The high cost and time claim of synchrotron-based techniques do not allow carrying out systematic studies on this area. However, they demonstrated the usefulness of micro-X-Ray diffraction (and its combination with micro-chemical analyses). Fortunately, micro-mineralogical techniques are already available even at the laboratory level nowadays.

This study tried to reveal the assumed differentiation and variance of Fe phases among and within ferromanganese nodules. A large number of nodules were studied by electron probe microanalysis and micro-X-Ray diffraction from soil profiles characterized by different conditions of hydromorphism. We also aimed to relate the mineralogy of nodules to their fabric, type, and conditions of hydromorphism.

2. Materials and methods

2.1. Soil samples and preparation

Two Vertisol profiles near by Kisújszállás (KU) and Verpelét (VP), a Solonetz profile near by Püspökladány (PL), a Gleysol profile near by Zalaszentlászló (ZS), a Luvisol profile near by Szentpéterfölde (SP), and a Phaeozem profile near by Rábapaty (RP) were sampled by genetic horizons from soil pits. Description of the soil profiles was carried out according to the FAO guidelines (FAO, 2006), and they were classified using the WRB system (FAO, 2014) (see Table 1 for qualifiers). Hydromorphism was present in the studied soils due to shallow groundwater (profiles KU, ZS, PL), stagnant surface water (profiles VP, SP), and regular flooding (profile RP). The exact locations of the soil pits are shown in Fig. S1.

In the profiles ZS and VP, the ferromanganese nodules were present only in one single horizon, whereas they could be observed at wide depth intervals in the other profiles (Table 1). The nodules were separated from the > 1 mm fraction of the soils manually under the stereomicroscope. Uncrushed samples of 200 g were dispersed in 0.25 M Na_2CO_3 overnight, and then the > 1 mm fraction was wet-sieved and washed with distilled water (Gasparatos et al., 2005). For the micro-analytical studies, four to six nodules from each sample were selected, and they were set into epoxy resin (Araldite 2020) using vacuum impregnation (Struers Citovac). Then, the impregnated nodules were cut (Struers Minitom) to show a cross-section, and micro-polished (Struers LaboPol-5). For the electron microprobe analyses, the polished surfaces were coated with carbon (JEOL JFC 1200 fine coater).

Table 1
Major physicochemical properties of the studied soils. Nodules appeared in horizons indicated by bold characters. *Data were taken from Fuchs et al. (2011) for profile KU and Kátai et al. (2016) for profile PL. sm = smectite, ver = vermiculite, ill = illite, chl = chlorite, kao = kaolinite.

Horizon	Depth	pH	SOM	Carbonate	Silt	Clay	Fe	Mn	Clay minerals
	(cm)		(%)	(%)	(%)	(%)	(%)	(mg/kg)	
*Kisújszállás **(KU)** - Epigleyic Epistagnic Mollic Endocalcic **Vertisol** (Ferric. Humic. Hypereutric. Pellic)**									
A	0–25	6.80	2.1	n.d.	38.2	44.6	4.38	510	sm, ill, ill/sm, chl, kao
AB	25–55	7.60	1.3	n.d.	42.8	45	4.97	1062	sm, ill, ill/sm, chl, kao, chl/sm
B	55–85	8.10	–	15.3	41.1	45.7	5.37	1469	sm, ill, ill/sm, chl, kao, chl/sm
C	85–110	8.10	–	7.3	47.2	40.9	4.32	390	
*Zalaszentlászló **(ZS)** – Mollic Calcic **Gleysol** (Loamic. Aric)*									
A1	0–20	7.57	5.5	1.0	44.1	15.8	2.91	744	
A2	20–55	8.06	1.4	6.3	30.4	23.1	3.04	1546	chl, ill
B	55–90	8.43	0.5	34.7	34.6	17.1	3.11	1112	
C	90–110	–	–	–	–	–	1.98	418	
*Püspölkadány **(PL)** - Vertic Endosalic Mollic Endogleyic Epistagnic **Solonetz** (Clayic. Hypernatric)**									
A	0–5	6.32	3.7	n.d.	39.8	28.5	2.80	527	
B1	5–30	6.77	1.8	n.d.	35.2	41.1	4.09	531	sm, ill, ill/sm, kao
B2	30–80	8.02	1.0	0.5	32.4	50.5	4.69	651	sm, ill, ill/sm, kao
BC	80–130	9.14	0.4	4.0	36.3	44.2	4.63	509	sm, ill, ill/sm, kao
C	130–160	9.26	0.2	4.0	36.7	50.5	7.45	1180	
*Verpelét **(VP)** – Pellic **Vertisol** (Aric. Gleyic)*									
A1	0–30	6.18	2.6	0.08	40.2	45.4	3.70	1017	
A2	30–65	6.51	1.7	0.04	36.6	51.1	3.97	965	sm, ill, kao
AB	65–80	7.06	1.3	0.08	37.1	52.3	4.03	1076	
*Szentpéterfölde **(SP)** – Endostagnic **Luvisol** (Loamic)*									
A	0–30	7.29	2.7	0.5	53.6	12.9	3.46	1111	
B	30–50	7.50	1.2	0.6	54.0	16.8	3.81	1161	
C1	50–67	7.42	0.5	0.1	51.0	29.9	4.53	648	chl/ver, ill/ver, ill, kao
C2	67–120	7.42	0.5	0.1	41.4	32.7	4.71	523	chl/ver, ill/ver, ill, kao
C3	120–150	6.68	0.2	0.1	43.1	30.7			
*Rábapaty **(RP)** – Stagnic Fluvic **Phaeozem** (Loamic. Aric)*									
A1	0–15	7.89	3.0	0.4	11.2	36.3	5.19	688	
A2	15–35	7.88	2.7	0.4	11.0	36.9	4.58	644	ver, chl/ver, ill, ill/ver, chl, kao
B	35–50	7.97	1.6	0.4	13.2	38.6	5.69	1192	ver, chl/ver, ill, ill/ver, chl, kao
C1	50–75	7.95	1.0	0.5	12.0	35.7	6.05	1409	ver, chl/ver, ill, ill/ver, chl, kao
C2	75–110	7.98	0.8	0.3	10.2	31.3	5.99	1511	ver, chl/ver, ill, ill/ver, chl, kao

For their physicochemical characterization, the soil samples were air-dried, gently crushed, and dry-sieved with a 2000 μm mesh size. Macroscopic traces of organic matter (roots, chaffs, debris, etc.) were removed physically. For the bulk mineralogical analyses, the soil samples and part of the separated nodules were gently crushed in an agate mortar. For the chemical analyses, the samples were grounded to a fine powder (10 μm). The clay fractions of the samples were separated by sedimentation in an aqueous suspension. Diagnostic treatments were carried out on the clay fractions to identify their clay mineral species after Harris and White (2008).

2.2. Soil analysis and analytical methods

The soil physical and chemical analyses were carried out according to standard methods (see more details in Makó and Tóth, 2013). The pH was measured in soil–water suspension at a ratio of 1:2.5 by the potentiometric method (Mclean, 1982). The organic matter content was determined by wet combustion with the Tyurin titrimetric method (Nelson and Sommers, 1996). The calcium carbonate content was studied by the Scheibler calcimeter (Nelson, 1982). The conventional sieve-pipette method was used to measure the particle-size distribution of the soils (Gee and Bauder, 1986).

The bulk soil samples, clay fractions, and powdered bulk nodules were studied for their mineralogy with a Rigaku Miniflex 600 X-Ray diffractometer at 40 kV and 15 mA using Cu Kα radiation. For bulk soil and nodule samples, the powdered material was loaded into steel holders to obtain random powder mounts, whereas clay fractions were mounted onto glass plates for analysis. The 2Θ range was set to 2–70° for bulk samples, and to 2–35° for the clay fractions. A counting speed of 0.05°/2 s was used for the analyses. For the qualitative analysis, the Rigaku PDXL2 software was used for phase identification based on the ICDD database. For the quantitative analysis of the bulk nodules, the diffraction patterns were processed using the Siroquant V4 software and the modal contents were determined by the Rietveld method.

Total Fe and Mn concentrations of the bulk soils and the powdered nodules were analyzed by a Spectro XSort Combi energy dispersive X-Ray fluorescence spectrometer.

The external and internal appearance of the nodules was characterized under a stereomicroscope. Micro-analytical analyses were carried out on the polished surface of 59 nodules. Electron-probe microanalysis was used to analyze the nodules' micro-fabric and the distribution of the major chemical elements (primarily Fe and Mn) within the nodules. Altogether 50 elemental distribution maps and 660 point and area analyses were carried out using a JEOL Superprobe JCXA-733 instrument equipped with an Oxford Instruments Inca energy 200 energy dispersive spectrometer. An acceleration voltage of 20 kV, a probe current of 6 nA were used for the analyses. Documentation of the studied areas was carried out by backscattered electron micrographs. The diameter of the electron beam used for the micro-chemical analyses was 1 μm. The count time for the point analyses and elemental maps were set to 60 and 300 s, respectively. Evaluation of the chemical data was carried out using the AZTEc software.

Based on the results of the electron-probe microanalysis, 28 nodules were selected for the micro-mineralogical analyses. Such analyses were carried out at 155 points using a Rigaku D/Max Rapid II diffractometer. The instrument was operated with CuKα radiation generated at 50 kV and 0.6 mA. For the point analyses, a collimated X-Ray beam with a diameter of 100 μm was used, and the analysis time was set to 300 s. A built-in CCD camera was used to select the area of analysis and precise positioning of the sample at a downward angle of 45°. The detector system uses a curved image plate (IP) placed on the inner surface of a cylinder that surrounds the ω-axis at the center, allowing the recording of a 2D diffraction image over a broad 2θ range. The IP is read by a laser-scanning readout system. The 2DP Rigaku software was used to record the diffraction image from the laser readout. The plot was read into Rigaku PDXL 1.8 software for data interpretation.

3. Results

3.1. Soil properties

The studied soils exhibited diverse physicochemical properties (Table 1). They were mostly neutral and slightly alkaline in their pH. The organic matter content of the samples varied widely among the samples with the absence of extreme values. They were primarily fine-grained soils, and the nodules appeared mainly in their horizons with clay or clay-loam texture. Their Fe (3–6%) and Mn (0.05–0.15%) content was not high, even in the horizons containing the nodules. The ratio of Fe and Mn showed high variation within the profiles. In most cases, this ratio was less than 75 showing the higher enrichment of Mn than Fe compared to the upper continental crust. On the contrary, this ratio was higher than 75 in some cases (KUA, PL BC, SP C2). Goethite was the only crystalline Fe-oxyhydroxide phase identified in the bulk soils, sometimes in their clay fraction only. Concerning their clay mineralogy, swelling clay minerals, illite (and their mixed layer species) were primarily dominant. Smectite was characteristic in the profiles KU, PL, and VP, vermiculite in the profile RP, and chlorite/vermiculite in the profile SP. The profile ZS did not contain any swelling clay mineral but chlorite and illite only.

3.2. Bulk nodule properties

The nodules' major characteristics are summarized in Table 2, and their stereomicroscopic images are shown in Fig. S2. Two major nodule types were observed: small (<2 mm), rectangular or slightly rounded, light-colored (grey, light brown, and reddish-brown) nodules, and large (up to 5–10 mm) spherical, dark-colored (dark grey, brown and black) nodules. In profiles where spherical nodules are present in more than one single horizon (profiles KU, PL, RP), their frequency and size are higher in the lower horizons. This phenomenon was not observed for the rectangular nodules. Rectangular nodules were characteristic of the lower horizons (profiles KU, PL), or they were present together with the spherical ones (profiles VP, SP, RP), or they were absent in the soil (profile ZS). However, in the profile SP, spherical nodules were characteristic of the lower parts of the profile, whereas the rectangular ones also appeared in the upper soil horizons.

Iron and Mn concentration was significantly higher in the nodules than in the bulk soils (Table 2). The highest Fe concentrations were found in horizons where the largest spherical nodules were found with the highest frequency. Such a relationship was not observed for Mn. Enrichment of the Fe and Mn in the bulk nodules did not show any relationship. The highest Fe enrichment was found in the profiles ZS and PL, followed by the profile KU, whereas the lowest enrichment was found for the profiles VP, SP, and RP. In the profiles where nodules appeared in several horizons, Fe enrichment in the bulk nodules decreased with depth. Manganese showed the highest enrichment in the nodules of the profile PL, followed by the profiles SP, RP, and KU, whereas relatively low Mn enrichment was found in the profiles VP and ZS. There was no characteristic change in Mn enrichment with depth. The ratio of Fe and Mn was generally higher in the bulk soil than in the nodules.

The mineralogical composition of the bulk nodules is shown in Table 3, and the relating XRD patterns are shown in Fig. S3. Their major mineral components were the same as those found in the soil matrix (quartz, feldspars, mica, and carbonates). The pedogenic minerals (oxyhydroxides, clay minerals, and carbonates) were also present. No crystalline Mn-phases could be identified in the nodules by powder XRD. Goethite was the only Fe-oxyhydroxide phase, which could be identified unambiguously in the nodules. Besides goethite, the presence of ferrihydrite could also be supposed in some cases (in horizons KU A and AB, PL BC, VP A2, and SP C2) based on the elevated background and/or diffuse peaks at 2.5 and 1.5 Å. Goethite was the major component of the largest spherical nodules with concentrations between 25 and 41% (ZS

Table 2
Major characteristics of the nodules found in the studied soils. s. = slightly, r. = reddish, l. = light.

Horizon	Nodule types	Size	Shape	Color	Frequency	Bulk Fe (%)	Bulk Mn (%)
Kisújszállás (KU) - Vertisol							
A	concentric with core	< 5 mm	rounded	r. brown, black, grey	+	25.9	3.31
AB	concentric with core	< 5 mm	rounded	r. brown, grey	++	22.3	3.04
B	typic	< 2 mm	s. rounded, rectangular	l. brown, grey, black	++	13.5	2.57
Zalaszentlászló (ZS) - Gleysol							
A2	concentric	< 10 mm	rounded	grey, l. brown, r. brown	+++	28.1	3.61
Püspölkadány (PL) - Solonetz							
B1	concentric with core, typic	< 2 (5) mm	rounded	r. brown	+	36.7	1.21
B2	concentric with core, concentric	< 5 mm	rounded	black, r. brown	++	31.6	2.00
BC	typic, coated typic	< 5 mm	s. rounded, rectangular	black, r. brown	++	11.3	4.65
Verpelét (VP) - Vertisol							
A2	concentric, typic	< 1 mm	rounded, s. rounded, rectangular	black	++	11.3	0.93
Szentpéterfölde (SP) - Luvisol							
C1	typic	< 2 (5) mm	rounded, s. rounded	l. brown, r. brown, black	++	13.2	1.99
C2	typic, concentric	< 5 mm	rounded, s. rounded	l. brown, r. brown, black	++	9.98	3.23
Rábapaty (RP) - Phaeozem							
A2	concentric, typic	< 1 mm	rounded, s. rounded	l. brown, r. brown, grey, black	+	14.6	4.40
B	concentric, typic	< 3 mm	rounded	r. brown, black, l. brown	++	14.2	4.36
C1	typic, concentric	< 3 mm	rounded, s. rounded, rectangular	l. brown, grey, r. brown, black	++	11.2	4.01
C2	typic	< 3 mm	s. rounded, rectangular	r. brown, black, grey	++	8.29	2.61

A2, KU A, and AB). In these cases, 70–90% of the total Fe of the nodules was present as goethite. However, in most cases, goethite was only a minor component (below 15%) of the nodules despite large spherical nodules (e.g., in soil PL B1, where goethite accounted for 24% of the total Fe in the bulk nodules). In some cases (horizons KU B, PL BC, SP C2), minor goethite (below 15%) was also found in the rectangular nodules. A large ratio of total Fe was present as goethite in the nodules of KU B and SP C2 horizons (70 and 95%, respectively) whereas this ratio (28%) was much lower in the nodules from the horizon PL BC. Contrarily, a low amount (well below 10%) of crystalline Fe-oxyhydroxide was found in the spherical nodules in certain soil horizons (PL B2, VP A2), with a relatively low ratio of goethite in the total Fe (below 30%). In the nodules of profile RP, Fe-oxyhydroxides could not be identified or only in a very low amount (3–4%), and a low ratio of goethite was found within the total Fe (below 30%).

3.3. Micro-properties – fabric, chemistry, mineralogy

Rectangular nodules did not show any characteristic fabric, and they could be classified as typic nodules (Fig. S2). In these nodules, relatively large and light-colored soil particles were cemented together by dark-colored and fine-grained material with no regular arrangement. In some cases, the edge of the nodules exhibited reddish color. In the BC horizon of the profile PL, a thin coating surrounded some typic nodules. One single typic nodule from the profile SP showed red color.

The spherical nodules exhibited concentric fabric. This fabric could be characteristic of the whole nodule on the one hand, or concentric layers were built up around a nucleus on the other. The fabric of the nucleus was similar to that of the typic nodules. The size of the nucleus could be as large as 2 mm. In small-sized concentric nodules, the nucleus may have total up to the majority of the nodule. The concentric layers were made up of fine-grained material, although the large soil particles were still present. The concentric layers were generally less than five, and their thickness was some tenth of millimeters. Their color was black, reddish-brown, or red. In some cases, the layers exhibited alternating color (for profiles KU, ZS, PL), whereas dark color may dominate in other ones (VP, SP, RP). The outermost layer was often reddish.

According to the backscattered electron images (shown in Figs. 1 and 2), there were both porous and compact nodules in both types. Pores and cavities may have been present in the nucleus or arranged to the concentric structure between the concentric layers. The porous character of the nodules may have shown variation even within a profile. For example, the nucleus of the nodules in the profile KU was porous in horizon A, whereas they were compacted in horizon B.

Manganese showed enrichment in the nucleus of the concentric nodules (Figs. 1 and 3). This metal formed distinct oxyhydroxide phases there in the form of pore or crack fillings. However, the concentric layers showed Fe enrichment, where the majority of the Fe-oxyhydroxides showed close association to silicates or even to Mn-oxyhydroxides. Distinct Fe-oxyhydroxide phases only appeared in the pore and crack fillings subordinately. The differentiation of Fe and Mn was the most conspicuous in the porous concentric nodules with a nucleus. Contrarily, Fe may also enrich in the nucleus of the compacted concentric nodules, and the Mn and Fe rich layers often showed alternation in the concentric part of these nodules. In the latter case, Mn tended to enrich in the internal part of the concentric layers, whereas Fe was enriched in the outer part. In the smaller concentric nodules (those in profiles VP, SP, RP), large, distinct Mn or Fe-oxyhydroxide fillings were less characteristic, and their association to silicates prevailed instead. The largest concentric nodules were compacted (profile ZS), and their interior consisted of well-separated, distinct Mn and Fe-oxyhydroxide phases. The dominance of Fe was also characteristic outwards together with the association of Fe-oxyhydroxides to silicates. As a mineralogical curiosity, separate Ba-phases were observed in the concentric nodules of the profile PL, which formed along the cracks between the concentric layers.

Contrarily, no characteristic Fe and Mn distribution could be observed in the typic nodules (Figs. 2 and 4). The Fe and Mn oxyhydroxides were mostly associated with silicates in these nodules. Iron and Mn enrichment showed patchy distribution generally, but a slight enrichment of Fe could be observed in the nodules' outermost parts in some cases.

Iron phases identified by the micro-XRD analyses are summarized in Table 3. These analyses focused on the following spots within the nodules: (1) large (>0.1 mm), distinct Fe or Mn oxyhydroxide phases (as observed by EPMA), (2) spots contrasting in color (e.g., the variation of red, red-brown, and black layers), and (3) comparison of internal and external parts of the nodules. Although quantitative analysis of mineral components could not be carried out based on micro-XRD data, the intensity of characteristic peaks may suggest the relative amount of the phase in question. A further indication of the amounts of phases (e.g.,

Table 3
Summary of the X-Ray diffractometric analyses of the soils and nodules. BS = bulk soil, CF = clay fraction, goe = goethite, qtz = quartz, ill = illite, pl = plagioclase, fhy = ferrihydrite, chl = chlorite, cal = calcite, dol = dolomite, kfs = K-feldspar, kao = kaolinite, hem = hematite, n.d. = not detected.

	Soils Fe minerals in BS or CF	Ferromanganese nodules		
		Bulk mineralogy (numerals indicate phase concentration in %)	Fe minerals in internal parts	Fe minerals in external parts
Kisújszállás (KU) - Vertisol				
A	n.d.	qtz (30), goe (29), pl (14), ill (13), kao (13)	goe, hem?	goe
AB	goe (CF)	qtz (32), goe (25), ill (19), chl (12), pl (12)	goe, fhy?	goe, fhy?
B	goe (BS, CF)	qtz (36), ill (20), goe (15), chl (15), pl (13), cal (1)	goe	goe
Zalaszentlászló (ZS) - Gleysol				
A2	goe (CF)	goe (41), qtz (32), cal (15), pl (6), ill (6), chl?	goe	goe
Püspökadány (PL) - Solonetz				
B1	n.d.	qtz (32), ill (20), pl (14), goe (14), dol (11), ill/sm (4), kao + chl (5)	goe	goe
B2	n.d.	qtz (59), pl (15), ill (14), goe (7), kao (5)	goe	goe
BC	n.d.	qtz (57), pl (20), ill (12), kao (6), goe (5)	goe?, fhy?	goe?, fhy?
Verpelét (VP) - Vertisol				
A2	n.d.	qtz (65), pl (20), goe/fhy (5), sm (4), ill (3), kao (3)	fhy?	fhy?
Szentpéterfölde (SP) - Luvisol				
C1	goe (BS, CF)	qtz (70), ill (12), pl (8), kfs (7), chl (3)	goe	goe
C2	goe (CF)	qtz (52), goe (15), ill (12), pl (12), chl (6), kfs (3)	fhy? (hem)	(hem)
Rábapaty (RP) - Phaeozem				
A	goe (BS)	qtz (38), ill (21), chl (20), pl (17) goe (4)	goe?	goe
B	goe (BS)	qtz (40), ill (23), chl (22), pl (15)	goe	goe
C1	goe (BS)	qtz (38), ill (25), chl (25), pl (12)	goe	goe
C2	goe (BS)	qtz (38), ill (24), chl (19), pl (16), goe (3)	n.d.	goe?

major or minor) is only based on this relationship.

The major soil components were the dominant phases in the nodules, like quartz, feldspar, clay minerals, and carbonates. In the following, only the Fe phases will be in focus. Their identification was primarily based on the following peaks and characteristics: peak at 4.20–4.17 Å for goethite, peak at 3.69 Å for hematite, and elevated background and/or diffuse peaks at around 2.5 Å and 1.5 Å for ferrihydrite.

In large concentric nodules with a nucleus of the profile KU, goethite was shown in the nucleus and the concentric layers (Figs. S4 and S5). Its frequency was higher in the dark concentric layers and lower in the light-colored parts of the nucleus. In one of the nodules, where the concentric layers exhibited red color, the presence of hematite could be supposed. On the contrary, the identification of crystalline Fe-oxyhydroxide mostly failed in the large concentric nodules of the profile PL. The presence of goethite could be verified only at some spots. Goethite could be unambiguously identified as a major component in the nodules with a Fe-rich nucleus from the horizon B1 of this profile. Identification of barite was also successful in several nodules from this profile based primarily on the peaks at 3.45 and 3.10 Å (Fig. S6). On the contrary, in the smaller concentric nodules with nucleus (in the profiles VP and RP), Fe oxyhydroxide phases could not be identified unambiguously. Elevation of background suggesting the presence of ferrihydrite was observed in almost every studied nodule at single spots. These observations could also be applied to the concentric nodules without a nucleus (Figs. S4 and S7).

In the large concretions of the profile ZS, goethite is present as a major component. However, in the concretions of the profile PL and the smaller concretions of the other profiles, goethite could be identified only in a few spots. For the typic nodules (Figs. S4 and S8), goethite could also be identified in the profiles where this phase was the major component of the concentric nodules (profile KU). However, in profiles where goethite was only a minor component of the concentric nodules (profiles PL, VP, SP), typic nodules also contained a very low amount or no goethite. Exceptions were the single red typic nodule from the profile SP and the typic nodules of the profile RP. In the red typic nodule, hematite was identified as a major Fe mineral. In the horizons A2, B, and C1 of the profile RP, goethite could be unambiguously identified in the typic nodules, whereas its presence is sporadic in horizon C2. Besides the Fe phases, Mn minerals could not be detected with these analyses, although several spots representing a phase composed of Mn and O solely were analyzed.

4. Discussion

4.1. Nodule types and conditions of hydromorphism

In the studied soils, hydromorphism was due to shallow groundwater table (in profiles KU, PL, ZS), stagnant surface water (in profiles VP, SP), or regular flooding (in profile RP). In all three cases, similar nodule types were formed with similar vertical distribution characteristics. The large concentric nodules formed in the zone of the most intense water oscillation. Concentric nodules also formed above this zone with smaller size and lower frequency, whereas the small typic nodules were characteristic below this zone. If the water oscillation zone is relatively narrow (like in profile ZS), large concentric nodules formed exceptionally. In this latter case, water oscillation could be very intense, as shown by the large size of the nodules and numerous concentric bands.

These nodule types are generally found in hydromorphic soils (Palumbo et al., 2001; Timofeeva et al., 2014). Their quantity, size, chemical composition, and micromorphology may vary with genetic horizons. These differences were related to different pedogenic stages (Sun et al., 2018). The nodules' banded structure likely formed in response to seasonal wetting and drying as an accretionary process. Shorter periods of reduction may result in the absence of some of the intermediated stages (Gasparatos et al., 2019). Additionally, Jien et al. (2010) reported that higher organic matter in the surrounding soil leads to smaller nodules. Eusterhues et al. (2008) observed that even small amounts of organic matter could influence the particle size and structural order of ferrihydrite. Additionally, low crystalline hydrous Fe-oxides are more prone to re-dissolution at reducing conditions. These conditions favor the formation of less developed concentric nodules in the upper part of the soil (above the zone of the most intense water oscillation). Contrarily, long periods of reduction do not allow concentric nodules to develop. However, the nodules' oxidization potential may inhibit the complete re-dissolution of Fe-oxyhydroxides (Sun et al., 2018). That is why typic nodules are characteristic of the deep layers of the profiles.

The observed nodule distribution was the most obvious in the soils with shallow groundwater table. In the other soil types, nodules could be characterized by smaller size, lower Fe enrichment, and higher frequency of non-crystalline Fe-oxyhydroxides in the bulk nodules, which could be related to the lower intensity of water oscillation and shorter redox periods. According to Timofeeva et al. (2014), well-developed morphological features, high differentiation and enrichment of Fe and Mn, and crystalline Fe-oxyhydroxides were characteristic of large nodules. However, Fe and Mn do not always show differentiation, and crystalline Fe-oxyhydroxides are sometimes absent in concentric nodules. Yu and Lu (2016) explained this phenomenon by the rapid changes in the soil's redox potential. Conditions of hydromorphism relate to the rate and intensity of redox changes resulting in differences in nodule development as found in our case. Nevertheless, the development of the

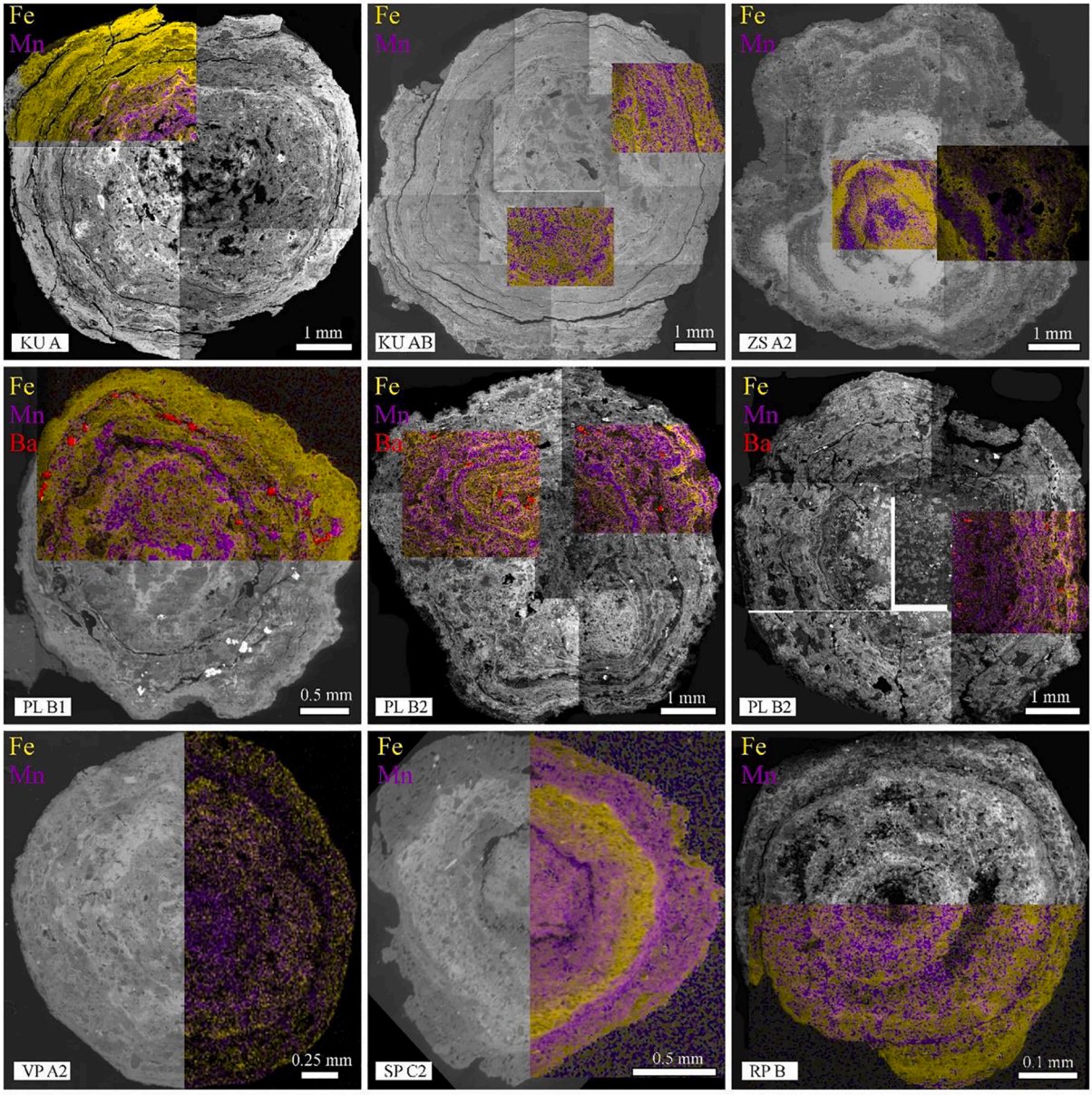

Fig. 1. Backscattered electron photomicrographs and Fe (yellow) and Mn (violet) elemental maps of characteristic concentric nodules. The red color shows Ba enrichment spots. (For interpretation of the references to colour in this figure legend, the reader is referred to the web version of this article.)

nodules' fabric showed the same characteristics in each case. Their fabric was not affected by the later ongoing crystallization of the Fe-oxyhydroxides, which needs favorable redox oscillation conditions.

In some cases, the concentric structure of the nodules was formed around a nucleus. These nodules may have been formed by the progression of typic nodules to concentric ones. In such cases, the relocation of the water oscillation zone can be supposed. Relocation is also probable when the presence of typic and concentric nodules was observed within the same horizon. Besides the relocation of the water oscillation zone, the nodules' transportation from other horizons can be assumed. In the first case, Fe-oxyhydroxide mineralogy of the different nodule types did not show any significant differences (like in profiles PL and RP). In the latter one, however, the nodules could show completely different Fe mineralogy, like in the case of the hematitic nodule in the profile SP. Hematite rarely occurs as the sole oxide in temperate soils. This mineral generally forms from a ferrihydrite precursor instead of goethite transformation (Bao and Koch, 1999). Low moisture content may favor ferrihydrite's dehydration to hematite over goethite (Zhang et al. 1998). The relatively high organic matter content of the subsoil may also facilitate this process (Kämpf and Schwertmann, 1983). The nodule with hematite probably represents a relict formation in our case.

4.2. *Nodule types and hydrous Fe oxide mineralogy*

The large concentric nodules enriched Fe the most, and they contained crystalline Fe-oxyhydroxides as a major component, primarily goethite. The EPMA analyses also supported these characteristics, as relatively large precipitations of Fe-oxyhydroxides were observed without any association to other phases. Contrarily, in those concentric nodules where such precipitations were associated with silicates (like in profile PL), goethite could be identified only as a minor component unless it was not present at all. Some concentric nodules with a nucleus could be characterized by a high Fe enrichment in the nucleus, whereas others in the concentric bands. Crystalline Fe-oxyhydroxide (goethite) was found primarily in those parts where high Fe enrichment was observed, despite Fe enrichment spots in parts with no crystalline Fe-

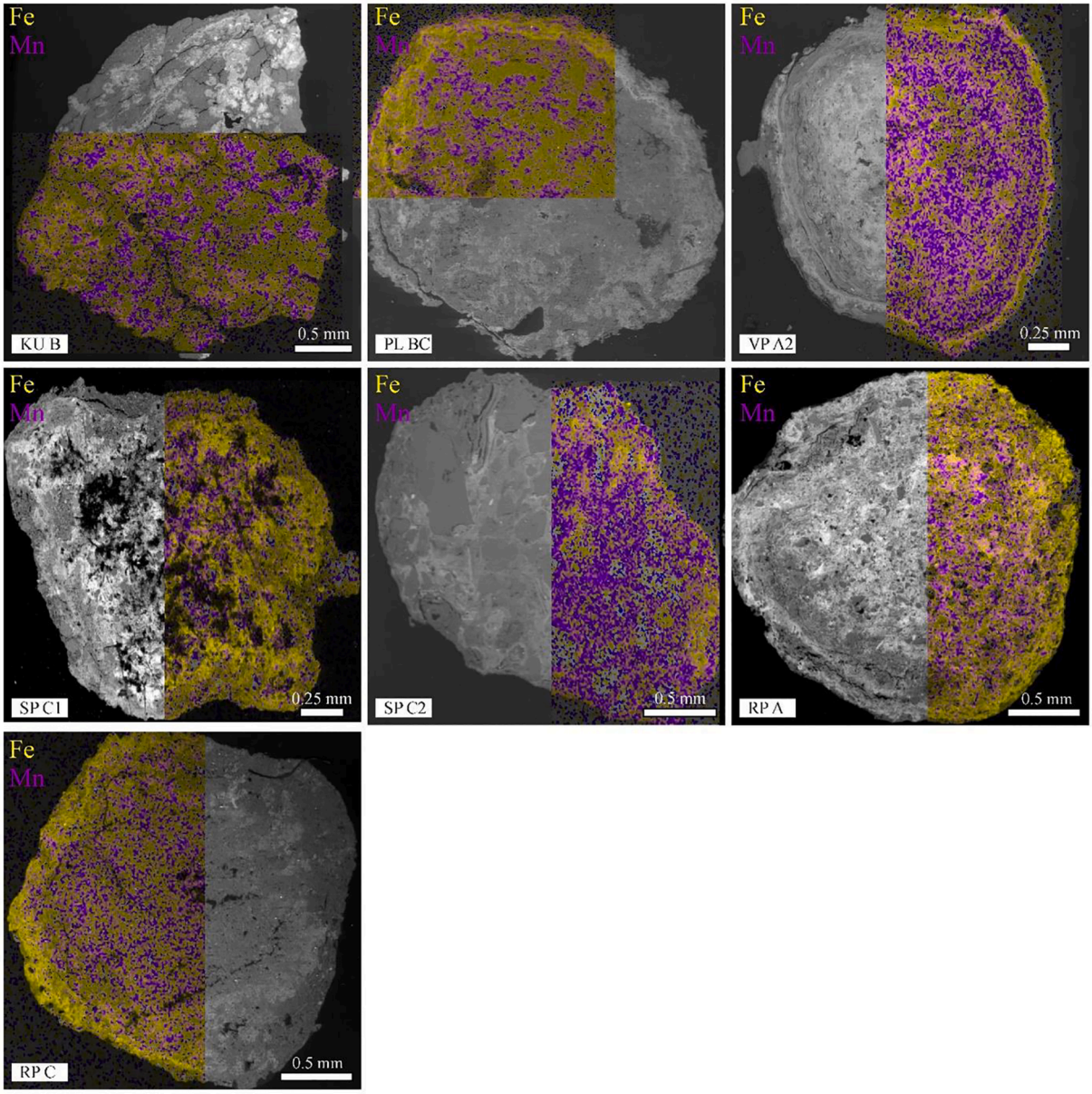

Fig. 2. Backscattered electron photomicrographs and Fe (yellow) and Mn (violet) elemental maps of characteristic typic nodules. (For interpretation of the references to colour in this figure legend, the reader is referred to the web version of this article.)

oxyhydroxides.

According to Thompson et al. (2006), redox oscillations can increase the crystallinity of hydrous Fe-oxides. Crystalline hydrous Fe-oxides may enrich through residual enrichment, which is due to the preferential dissolution of weakly crystalline hydrous Fe-oxides under reducing conditions (Bonneville et al., 2009), or through the catalytic reaction of released Fe(II) under anoxic conditions (Boland et al., 2014). During this process, mineral dissolution and subsequent re-crystallization occur. Large-sized nodules may have an oxidization potential high enough to inhibit the re-dissolution of Fe-oxyhydroxides. However, the crystallization may still proceed due to the soil solution reaching the nodules' interior through their pore system (Sun et al., 2018).

The large concentric nodules formed within the most intense water oscillation zone favor the Fe-oxyhydroxide crystallization due to the processes described above. The crystallization of ferrihydrite into more crystalline phases is strongly inhibited by organic matter and dissolved Si and Al (Jones et al., 2009). Schwertmann et al. (2000) observed that smectite and less crystalline silicates (like allophane) impeded ferrihydrite's crystallization in the long term. The inhibitory effect could be due to the Si accumulation on the ferrihydrite surface from the low-crystalline clay phases. The first Fe-oxyhydroxide precipitates may catalyze the further formation of such phases as coatings while the crystallization of the former still takes place. If the later generation of Fe-oxyhydroxides shows a strong association with silicates, a low-Fe coating will form around a high-Fe nucleus. Aggregates consisting of primary soil particles, clay minerals, and Fe-oxyhydroxides may also be coated by Fe-oxyhydroxide material dominantly. The further enrichment of the coating bands is the result of the subsequent precipitation events. The joint presence of low-Fe and high-Fe coating bands on the nodules of the same horizon may suggest the variation in Fe supply or the differences in catalyzing potential of a nodule with significantly different Fe-oxyhydroxide content. As shown by Vogelsang et al. (2016), intermittent drainage and waterlogged conditions may cause the destruction of clay minerals in paddy soils. If this process is more characteristic within the nodules than in the bulk soil, the low crystallinity of clay minerals could also affect the crystallization process of the

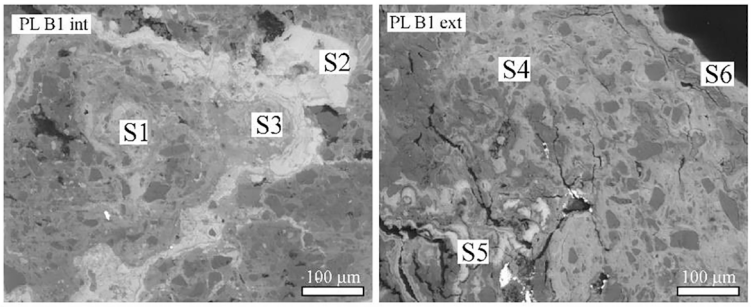

	O	Si+Al	Mn	Fe	Ba
S1	23.06		56.71		
S2	20.49		56.79		7.33
S3	28.55	12.88	5.56	38.19	

	O	Si+Al	Mn	Fe	Ba
S4	19.50		54.17		13.58
S5	30.34	16.96		41.28	
S6	23.82	5.58		59.74	

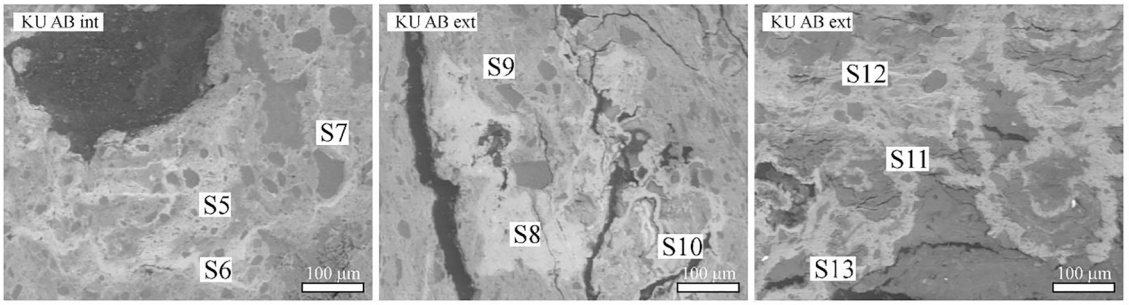

	O	Si+Al	Mn	Fe	Ba
S5	27.87	14.71	33.79		7.64
S6	22.19		22.05	38.86	
S7	22.00		19.20	43.49	

	O	Si+Al	Mn	Fe	Ba
S8	23.14	4.70	4.52	56.68	
S9	29.27	15.21		43.25	
S10	18.57		56.43		13.52

	O	Si+Al	Mn	Fe	Ba
S11	28.68	14.08		46.29	
S12	21.69		6.93	58.23	
S13	22.67			62.20	

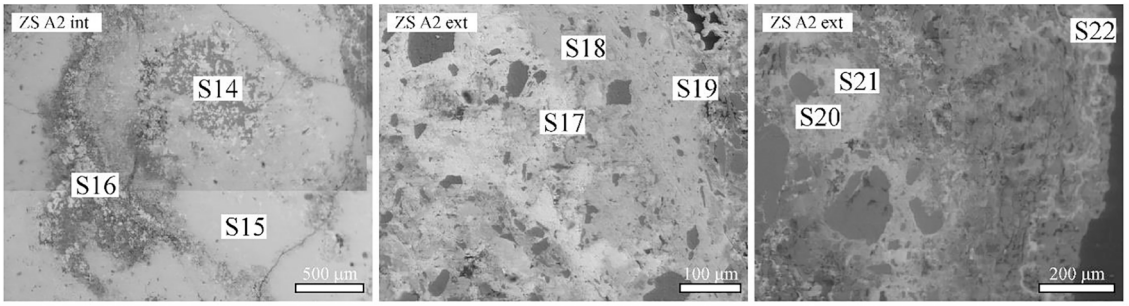

	O	Si+Al	Mn	Fe	Ba
S14	18.13		53.49		16.90
S15	21.28			61.10	
S16	18.26		49.80		16.49

	O	Si+Al	Mn	Fe	Ba
S17	24.56	10.16	38.31		12.35
S18	22.17		19.35	41.08	
S19	23.78	5.92		54.99	

	O	Si+Al	Mn	Fe	Ba
S20	19.25		52.51		12.03
S21	23.51	5.72	17.96	37.71	
S22	31.58	18.81		34.81	

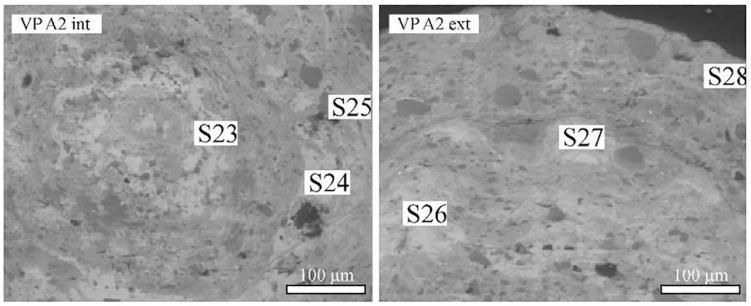

	O	Si+Al	Mn	Fe	Ba
S23	21.05		51.90	6.03	5.58
S24	20.82		53.11	6.78	5.21
S25	31.75	18.30	12.77	24.99	

	O	Si+Al	Mn	Fe	Ba
S26	22.69		28.69	29.75	
S27	22.57		41.90	14.83	
S28	30.10	15.10		37.74	

Fig. 3. Characteristic micro-fabric and distribution characteristics of Fe and Mn phases in the concentric nodules.

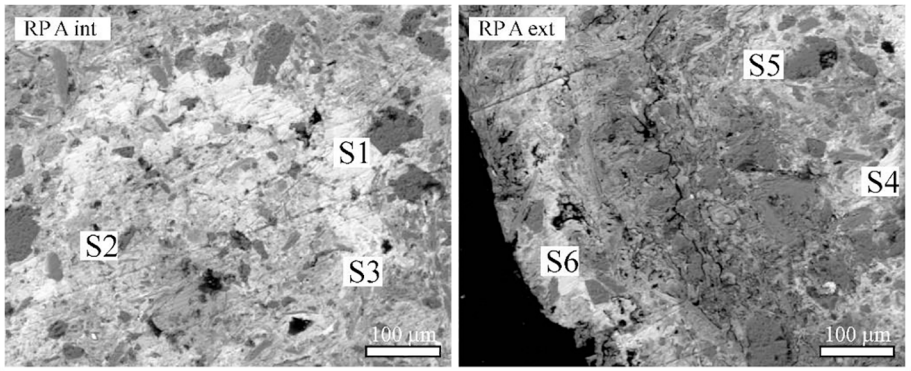

	O	Si+Al	Mn	Fe	Ba		O	Si+Al	Mn	Fe	Ba
S1	22.84		23.14	33.86		S4	21.62		38.59	19.11	
S2	32.77	19.56		32.61		S5	31.92	17.88	10.83	20.94	
S3	20.37		49.92	5.86	8.43	S6	28.41	13.79		42.41	

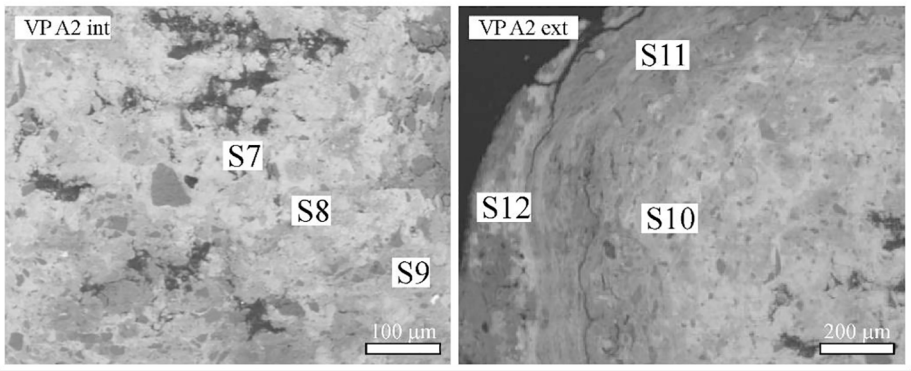

	O	Si+Al	Mn	Fe	Ba		O	Si+Al	Mn	Fe	Ba
S7	21.24		51.47	6.23	4.93	S10	31.40	18.76	26.92	7.33	
S8	34.80	23.26	4.76	25.10		S11	31.46	18.97	27.34	7.38	
S9	21.08		52.99		5.78	S12	29.06	12.85	12.72	31.91	

Fig. 4. Characteristic micro-fabric and distribution characteristics of Fe and Mn phases in the typic nodules.

Fe-oxyhydroxides.

Typic nodules contained crystalline Fe-oxyhydroxides only in soils with the most intense hydromorphism. However, in other soils, crystalline phases were not observed in such nodules, although they contained significant Fe enrichment spots. As typic nodules appeared below the most intense water oscillation zone, they were preferably exposed to re-dissolution due to the prolonged waterlogging. These conditions inhibited the development of a concentric structure and often the crystallization of Fe-oxyhydroxides. Vogelsang et al. (2016) explained the trend of increasing portions of less crystalline goethite in paddy soils by either insufficient time for re-crystallization of ferric precipitates and/or the decrease in crystal size of Fe-oxyhydroxides present upon partial reductive dissolution. Although concentric nodules do not necessarily contain crystalline Fe-oxyhydroxides, the duration of waterlogging plays a significant role in the nodule formation, besides the intensity of water oscillation. For example, Chen et al. (2019) observed differences in (hydrous) Fe-oxide crystallinity within redoximorphic soils. They explained this difference by the different timescale of Fe redox cycling or differences in processes affecting the crystallization of such phases.

4.3. Role of clay minerals in nodule formation

The clay content of the studied soils is mostly between 30 and 50%, and their clay mineralogy is dominated by swelling clay minerals, illite, and their mixed-layer variants. The only exception is the profile ZS, where the clay content is between 15 and 25%, and chlorite and illite were identified. In this profile, the large concentric nodules appeared in a narrow depth interval suggesting a significant external Fe supply. Soil chlorite is generally inherited from the parent material, although its formation is also hypothesized through hydroxy-interlayering of layer silicates by ferrolysis under alternating redox conditions (Georgiadis et al., 2020). Chlorite weathering could have been the source of Fe in this soil, but its pedogenic formation is also possible.

Clay content and mineralogy of soils can be strongly related to hydromorphic conditions. Nodules occur most frequently in fine-textured (silt- or clay-rich) soils with restricted permeability or poor drainage (Stiles et al., 2001). The oscillating water table promotes the formation and downward migration of secondary phases, often leading to seasonal water ponding. The fluctuation of base cation concentrations also favors the formation of clay minerals through metastable precursor mixed-layer clays (Thananchit et al., 2006). The varying redox conditions affect the layer charge of these phases, determining the type of base cation entering their structure (Stucki, 2013). Transformation of the inherited clay minerals may be incomplete under hydromorphic conditions, and together with the newly formed metastable precursor, they could simultaneously weather into stable species (Hong et al., 2015). That is why several clay minerals and their mixed-layer variants could be identified in the studied soils.

The formation of (swelling) clay minerals may promote the Fe-oxyhydroxide formation by inhibiting the water circulation and enhancing soil–water interaction. Additionally, their large surface area and charged surface support a suitable medium for the initial precipitation of hydrous Fe-oxides. Van Groeningen et al. (2020) demonstrated in laboratory experiments that surface-mediated oxidation of ferrous

ions may occur under anoxic conditions in the presence of smectite at neutral to alkaline pH. Their Mössbauer and XAS analyses also showed that subsequent aeration led to the complete oxidation of sorbed iron and the formation of Fe(III) phases, like Fe-bearing clay minerals, ferrihydrite, and lepidocrocite. The alkalinity of the studied soils must have neutralized the exchangeable H^+ formed at the same time. Consequently, ferrolysis could not result in strong acidification, and smectite, vermiculite, illite, and mixed-layer species represent the stable clay mineral phases in the studied soils. As Fe in the clay minerals also undergoes redox reactions, the physicochemical properties of clay minerals and their surrounding matrix will change (Pentráková et al., 2013). The reduction of Fe in smectite clays usually induces mixed-layer illite–smectite formation (Zhang et al., 2012). On the contrary, Fe reduction in illite may lead to increased layer charge, and the incomplete reoxidation of reduced Fe may cause illite to smectite transition (Huggett and Cuadros, 2005). Clay minerals may support the surface for the initial formation of Fe-oxyhydroxides, which is the first step in the nodule formation (Sipos et al., 2016). Although the same types of clay minerals could be identified in the nodules as in the bulk soils, the prevalence of illite seemed to be higher in the nodules than in the bulk soils. Authigenic clay phases may have been formed from the inherited crystalline illite (and chlorite). Their crystallization was more restricted in the nodules than in the soil matrix due to the redox reactions described above. However, the explanation of clay minerals' exact role in nodule formation needs further detailed studies in these (and in other hydromorphic) soils.

4.4. Barite in ferromanganese nodules

A novel finding of this study was identifying barite in the concentric nodules of the profile PL. This Ba-sulfate mineral is relatively rare in soils. It is mostly related to the salt-affected soils (Doner and Grossl, 2002), especially to hydromorphic conditions and saline groundwater (Bullock et al., 1985). The profile PL is a Solonetz, where salt accumulation arises from confinement, created by the subsoil clay accumulation to water flow out and evaporate. Earlier studies on nodules found that Ba is generally enriched in the Mn-oxyhydroxides within the nodules (e.g., Ettler et al., 2017). We also found up to 14.46% Ba in the Mn-rich precipitations in the studied nodules. However, in the profile PL, Ba formed a separate phase whereas still enriched with Mn-oxyhydroxides (up to 11.45%). According to Dixon and White (2002), only very low Ba concentrations may be held in crystal imperfections of Mn-oxyhydroxides. The high Ba concentration suggests that this element is held in the nodules as rare crystals of hollandite, a barium-manganese oxide mineral. In the profile PL, the barite is an authigenic phase. It could be observed along the cracks between the concentric bands of the nodules. Consequently, its formation took place with that of the nodules simultaneously when precipitation of hydrous Fe and Mn oxides were intermitted temporarily. At his stage of the nodule formation, barite precipitated in the presence of excess sulfate in the soil solution due to the saline environment.

5. Conclusions

Different conditions of hydromorphism resulted in the same nodule types and their similar vertical distribution in soils. Concentric nodules developed within and above the zone of the most intense water oscillation. Typic nodules were characteristic below this zone. These characteristics were the most obvious in the soils with shallow groundwater table. Contrarily, nodules showed smaller size, lower Fe enrichment, and the dominance of non-crystalline hydrous Fe oxides in soils with regular flooding and stagnant surface water. This difference could be related to the lower intensity of water oscillation and the shorter redox periods in the latter soils.

These two conditions affected the development of the nodules' fabric, which generally preceded the crystallization of hydrous Fe oxides. Relocation of the water oscillation zone within the soil may have resulted in different nodule types within the same layer or the formation of concentric nodules with a typic nucleus.

The largest concentric nodules formed within the most intense water oscillation zone favoring the Fe enrichment and Fe-oxyhydroxide crystallization the most. The hydrous Fe oxides did not show any differentiation within the nodules. Their association to (low crystalline?) clay minerals, however, may have also affected the crystallization process within the nodules. Although slight differences between the clay mineralogy of the nodules and bulk soils could be observed, this relationship needs further detailed studies. As a mineralogical curiosity, barite formation was observed in the nodules of the Solonetz profile. Authigenic barite formation took place in the presence of excess sulfate in the soil solution due to the saline environment, when precipitation of hydrous Fe and Mn oxides were temporarily intermitted.

Declaration of Competing Interest

The authors declare that they have no known competing financial interests or personal relationships that could have appeared to influence the work reported in this paper.

Acknowledgments

This study was supported by the European Union and the State of Hungary, co-financed by the European Regional Development Fund (GINOP-2.3.2-15-2016-00009 "ICER"), and by the Hungarian National Research, Development and Innovation Office (K 119475). Adrienn Tóth is grateful for the support of the János Bolyai Research Scholarship of the Hungarian Academy of Sciences. The authors thank the two anonymous reviewers for their useful comments and suggestions.

Appendix A. Supplementary data

Supplementary data to this article can be found online at https://doi.org/10.1016/j.geoderma.2021.115445.

References

Aide, M., 2005. Elemental composition of soil nodules from two Alfisols on an alluvial terrace in Missouri. Soil Sci. 170, 1022–1033. https://doi.org/10.1097/01.ss.0000187351.16740.55.

Bao, H., Koch, P.L., 1999. Oxygen isotope fractionation in ferric oxide-water systems: low temperature synthesis. Geochim. Cosmochim. Acta 63, 599–613. https://doi.org/10.1016/S0016-7037(99)00005-8.

Boland, D.D., Collins, R.N., Miller, C.J., Glover, C.J., Waite, T.D., 2014. Effect of solution and solid-phase conditions on the Fe(II)-accelerated transformation of ferrihydrite to lepidocrocite and goethite. Env. Sci. Technol. 48, 5477–5485. https://doi.org/10.1021/es4043275.

Bonneville, S., Behrends, T., Van Cappellen, P., 2009. Solubility and dissimilatory reduction kinetics of iron(III) oxyhydroxides: a linear free energy relationship. Geochim. Cosmochim. Acta 73, 5273–5282. https://doi.org/10.1016/j.gca.2009.06.006.

Bullock, P., Fedoroff, N., Jongerius, A., Stoops, G., Tursina, T., 1985. Handbook for Soil Thin Section Description. Waine Research, Wolverhampton.

Chen, C., Barcellos, D., Richter, D.D., Schroeder, P.A., Thompson, A., 2019. Redoximorphic Bt horizons of the Calhoun CZO exhibit depth-dependent iron-oxide crystallinity. J. Soils Sediments 19, 785–797. https://doi.org/10.1007/s11368-018-2068-2.

Cheng, Y.-Q., Yang, L.-Z., Cao, Z.-H., Ci, E.n., Yin, S., 2009. Chronosequential changes of selected pedogenic properties in paddy soils as compared with non-paddy soils. Geoderma 151, 31–41. https://doi.org/10.1016/j.geoderma.2009.03.016.

Cornell, R.M., Schwertmann, U., 2003. The Iron Oxides. Wiley-VCH, Weinheim, FRG.

Cornu, S., Deschatrettes, V., Salvador-Blanes, S., Clozel, B., Hardy, M., Branchut, S., Le Forestier, L., 2005. Trace element accumulation in Mn-Fe-oxide nodules of a planosolic horizon. Geoderma 125, 11–24. https://doi.org/10.1016/j.geoderma.2004.06.009.

Dixon, J.B., White, G.N., 2002. Manganese oxides. in: Dixon, J.B:, Schulze, D.G. (Eds.), Soil mineralogy with environmental applications, SSSA Book series, No. 7, SSSA, Madison, pp. 367-388.

Doner, H.E., Grossl, P., 2002. Sulfides and sulfates. in: Dixon, J.B:, Schulze, D.G. (Eds.), Soil mineralogy with environmental applications, SSSA Book series, No. 7, SSSA, Madison, pp. 229-260.

Ettler, V., Chren, M., Mihajlevic, M., Drahota, P., Kribek, B., Veselovsky, F., Sracek, O., Vanek, A., Penizek, V., Komarek, M., Mapani, B., Kamona, F., 2017. Characterization of Fe-Mn concentric nodules from Luvisol irrigated by mine water in a semi-arid agricultural area. Geoderma 299, 32–42. https://doi.org/10.1016/j.geoderma.2017.03.022.

Eusterhues, K., Wagner, F.E., Häusler, W., Hanzlik, M., Knicker, H., Totsche, K.U., Kögel-Knabner, I., Schwertmann, U., 2008. Characterization of ferrihydrite-soil organic matter coprecipitates by X-ray diffraction and Mössbauer spectroscopy. Environ. Sci. Technol. 42, 7891–7897. https://doi.org/10.1021/es800881w.

FAO, 2006. Guidelines for soil description. Food and Agriculture Organization of the United Nations, Rome.

FAO, 2014. World reference base for soil resources. International soil classification system for naming soils and creating legends for soil maps. World Soil Resources Reports No. 106. Food and Agriculture Organization of the United Nations, Rome.

Fuchs, M., Szegi, T., Láng, V., 2011. Útmutató a Magyarország talajai talajtani szakmérnöki tárgy tanulmányútjához, Szent István Egyetem, Talajtani és Agrokémiai Tanszék.

Gasparatos, D., Tarenidis, D., Haidouti, C., Oikonomou, G., 2005. Microscopic structure of soil Fe-Mn nodules: environmental implication. Environ. Chem. Lett. 2, 175–178. https://doi.org/10.1007/s10311-004-0092-5.

Gasparatos, D., Massas, I., Godelitsas, A., 2019. Fe-Mn concretions and nodules formation in redoximorphic soils and their role on soil phosphorus dynamics: current knowledge and gaps. Catena 182, 104106. https://doi.org/10.1016/j.catena.2019.104106.

Gee, G.W., Bauder, J.W., 1986. Particle-size analysis. in: Klute, A. (Ed.), Methods of Soil analysis, Part 1, Physical and Mineralogical Methods. SSSA Book Series, No. 1, SSSA, Madison, pp. 383-411. doi:10.2136/sssabookser5.1.2ed.c15.

Georgiadis, A., Dietel, J., Dohrmann, R., Rennert, T., 2020. What are the nature and formation conditions of hydroxy-interlayered minerals (HIMs) in soil? J. Plant Nutr. Soil Sci. 183, 12-26. doi:10.1002/jpln.201900283.

Harris, W., White, N.G., 2008. X-ray diffraction techniques for soil mineral identification. in: Ulrey, A.L., Dress, R. (Eds.), Methods of Soil Analysis, Part 5, Mineralogical Methods. SSSA Book Series, No. 5, SSSA, Madison, pp. 81–116. doi:10.2136/sssabookser5.5.c4.

Hickey, P.J., McDaniel, P.A., Strawn, D.G., 2008. Characterization of iron-manganese cemented redoximorphic aggregates on Wetland soils contaminated with mine wastes. J. Environ. Qual. 37, 2375–2385. https://doi.org/10.2134/jeq2007.0488.

Hong, H., Cheng, F., Yin, K.e., Churchman, G.J., Wang, C., 2015. Three-component mixed-layer illite/smectite/kaolinite (I/S/K) minerals in hydromorphic soils, south China. Am. Mineral. 100, 1883–1891. https://doi.org/10.2138/am-2015-5170.

Huggett, J.M., Cuadros, J., 2005. Low-temperature illitization of smectite in the late Eocene and early oligocene of the Isle of Wight (Hampshire basin), UK. Am. Mineral. 90, 1192–1202. https://doi.org/10.2138/am.2005.1674.

Jien, S.-H., Hseu, Z.-Y., Chen, Z.-S., 2010. Hydropedological implications of ferromanganiferous nodules in rice-growing plinthitic Ultisols under different moisture regimes. Soil Sci. Soc. Am. J. 74, 880–891. https://doi.org/10.2136/sssaj2009.0020.

Jones, A.M., Collins, R.N., Rose, J., Waite, T.D., 2009. The effect of silica and natural organic matter on the Fe(II)-catalysed transformation and reactivity of Fe(III) minerals. Geochim. Cosmochim. Acta 73, 4409–4422. https://doi.org/10.1016/j.gca.2009.04.025.

Kämpf, N., Schwertmann, U., 1983. Goethite and hematite in a climosequence in southern Brazil and their application in classification of kaolinitic soils. Geoderma 29, 27–39. https://doi.org/10.1016/0016-7061(83)90028-9.

Kátai, J., Michéli, E., Dobos, E., Sándor, Z.s., Tállai, M., Csiha, I., Rásó, J., Balla, D., Novák, T.J., 2016. Okszerű talajhasználat – Talajvédelem, Kirándulásvezető a terepi programhoz, Talajtani Vándorgyűlés 2016. Magyar Talajtani Társaság, Debreceni Egyetem.

Kölbl, A., Schad, P., Jahn, R., Amelung, W., Bannert, A., Cao, Z.-H., Fiedler, S., Kalbitz, K., Lehndorff, E., Müller-Niggemann, C., Schloter, M., Schwark, L., Vogelsang, V., Wissing, L., Kögel-Knabner, I., 2014. Accelerated soil formation due to paddy management on marshlands (Zhejiang Province, China). Geoderma 228-229, 67–89. doi:10.1016/j.geoderma.2013.09.005.

Makó, A., Tóth, B. 2013. Soil data from Hungary, in: Weynants, M. (Ed.), European Hydropedological Data Inventory (EU-HYDI). Publications Office of the European Union, JRC Technical Reports, Brussels. pp. 50–55.

Manceau, A., Tamura, N., Celestre, R.S., MacDowell, A.A., Geoffroy, N., Sposito, G., Padmore, H.A., 2003. Molecular-sclae speciation of Zn and Ni in soil ferromanganese nodules from loess soils of the Mississippi Basin. Env. Sci. Technol. 37, 75–80. https://doi.org/10.1021/es025748r.

McLean, E.O., 1982. Soil pH and lime requirement. in: Page, A. L., Miller, R.H., Keeny, D. R. (Eds.), Methods of soil analysis, Part 2, Chemical and Microbiological Properties, SSSA Book Series, No. 2, SSSA, Madison, pp. 199-224. doi:10.2134/agronmonogr9.2.2ed.c12.

Nelson, D.W., Sommers, L.E., 1996. Total carbon, organic carbon, and organic matter. in: Sparks, D.L., Page, A.L., Helmke, P.A., Loeppert, R.H., Soltanpour, P.N., Tabatabai, M.A., Johnston, C.T., Summer, M.E. (Eds.), Methods of Soil Analysis, Part 3, Chemical Methods, SSSA Book Series, No. 3, SSSA, Madison, pp. 961-1010. doi:10.2136/sssabookser5.3.c34.

Nelson, R.E., 1982. Carbonate and gypsum. in: Page, A. L., Miller, R.H., Keeny, D.R. (Eds.), Methods of soil analysis, Part 2, Chemical and Microbiological Properties, SSSA Book Series, No. 2, SSSA, Madison, pp. 181–197. doi:10.2134/agronmonogr9.2.2ed.c11.

Palumbo, B., Bellanca, A., Neri, R., Roe, M.J., 2001. Trace metal partitioning in Fe-Mn nodules from Sicilian soils. Italy. Chem. Geol. 173, 257–269. https://doi.org/10.1016/S0009-2541(00)00284-9.

Pentráková, L., Su, K., Pentrák, M., Stucki, J.W., 2013. A review of microbial redox interactions with structural Fe in clay minerals. Clay Miner. 48, 543–560. https://doi.org/10.1180/claymin.2013.048.3.10.

Ram, H., Singh, R.P., Prasad, J., 2001. Chemical and mineralogical composition of Fe-Mn concretions and calcretes occurring in sodic soils of Eastern Uttar Pradesh, India. Aust. J. Soil Res. 39, 641–648. https://doi.org/10.1071/SR98098.

Rhoton, F.E., Bigham, J.M., Schulze, D.G., 1993. Properties of iron-manganese nodules from a sequence of eroded Fragipan Soils. Soil Sci. Soc. Am. J. 57, 1386–1392. https://doi.org/10.2136/sssaj1993.03615995005700050037x.

Schwertmann, U., Friedl, J., Stanek, H., Schulze, D.G., 2000. The effect of clay minerals on the formation of goethite and hematite from ferrihydrite after 16 years' ageing at 25°C and pH 4–7. Clay Miner. 35, 613–623. https://doi.org/10.1180/000985500547034.

Šegvić, B., Girardclos, S., Zanoni, G., Arbiol González, C., Steimer-Herbet, T., Besse, M., 2018. Origin and paleoenvironmental significance of Fe-Mn nodules in the Holocene perialpine sediments of Geneva Basin, western Switzerland. Appl. Clay Sci. 160, 22–39. https://doi.org/10.1016/j.clay.2018.01.027.

Sipos, P., Balázs, R., Bozsó, G., Németh, T., 2016. Changes in micro-fabric and re-distribution of Fe and Mn with nodule formation in a floodplain soil. J. Soil Sediment 16, 2105–2117. https://doi.org/10.1007/s11368-016-1393-6.

Stiles, C.A., Mora, C.I., Driese, S.G., 2001. Pedogenic iron-manganese nodules in Vertisols: A new proxy for paleoprecipitation? Geology 29, 943-946. doi:10.1130/0091-7613(2001)029<0943:PIMNIV>2.0.CO;2.

Stucki, J.W., 2013. Properties and behavior of iron in clay minerals. in: Bergaya, F., Lagaly, G. (eds). Developments in Clay Science, Volume 5. Elsevier, pp. 559-611. doi:10.1016/B978-0-08-098258-8.00018-3.

Sun, Z.X., Jiang, Y.Y., Wang, Q.B., Owens, P.R., 2018. Fe-Mn nodules in a southern Indiana loess with a fragipan and their soil forming significance. Geoderma 313, 92–111. https://doi.org/10.1016/j.geoderma.2017.10.025.

Szymanski, W., Skiba, M., Blachowski, A., 2014. Mineralogy of Fe–Mn nodules in Albeluvisols in the Carpathian Foothills, Poland. Geoderma 217-218, 102-110. doi:10.1016/j.geoderma.2013.11.008.

Thananchit, S., Suddhiprakarn, A., Kheoruenromne, I., Gilkes, R.J., 2006. The geochemistry of soils on a catena on basalt at Khon Buri, northeast Thailand. Geoderma 135, 81–96. https://doi.org/10.1016/j.geoderma.2005.10.010.

Thompson, A., Chadwick, O.A., Rancourt, D.G., Chorover, J., 2006. Iron-oxide crystallinity increases during soil redox oscillations. Geochim. Cosmochim. Acta 70, 1710–1727. https://doi.org/10.1016/j.gca.2005.12.005.

Timofeeva, Y.O., Karabtsov, A.A., Semal', V.A., Burdukovskii, M.L., Bondarchuk, NataliaV., 2014. Iron-manganese nodules in Udepts: the dependence of the accumulation of trace elements on nodule size. Soil Sci. Soc. Am. J. 78, 767–778. https://doi.org/10.2136/sssaj2013.10.0444.

Van Groeningen, N., ThomasArrigo, L.K., Byrne, J.M., Kappler, A., Christl, I., Kretzschmar, R., 2020. Interactions of ferrous iron with clay mineral surfaces during sorption and subsequent oxidation. Environ. Sci.: Processes Impacts 22, 1355–1367. https://doi.org/10.1039/D0EM00063A.

Vepraskas, M.J., Vaughan, K.L., 2016. Morphological features of hydric and reduced soils. in: Vepraskas, M.J., Craft, CB (Eds.), Wetland soils. Genesis, hydrology, landscapes and classification, CRC Press, Boca Raton, pp. 190-219.

Vogelsang, V., Kaiser, K., Wagner, F.E., Jahn, R., Fiedler, S., 2016. Transformation of clay-sized minerals in soils exposed to prolonged regular alternation of redox conditions. Geoderma 278, 40–48. https://doi.org/10.1016/j.geoderma.2016.05.013.

White, G.N., Dixon, J.B., 1996. Iron and manganese in nodules from a young Texas Vertisol. Soil Sci. Soc. Am. J. 60, 1254–1262. https://doi.org/10.2136/sssaj1996.03615995006000040042x.

Yu, X., Lu, S., 2016. Micrometer-scale internal structure and element distribution of Fe-Mn nodules in Quaternary red earth of Eastern China. J. Soils Sediments 16, 621–633. https://doi.org/10.1007/s11368-015-1212-5.

Zhang, J., Dong, H., Liu, D., Fischer, T.B., Wang, S., Huang, L., 2012. Microbial reduction of Fe(III) in illite–smectite minerals by methanogen Methanosarcina mazei. Chem. Geol. 292-293, 35–44. doi:10.1016/j.chemgeo.2011.11.00.

Zhang, M., Karathanasis, D., 1997. Characterization of iron-manganese concretions in Kentucky Alfisols with perched water tables. Clay Clay Miner. 45, 428–439. https://doi.org/10.1346/CCMN.1997.0450312.